Available online at www.sciencedirect.com
ScienceDirect
Journal of Magnetic Resonance 183 (2006) 1–12
JMR Journal of Magnetic Resonance
www.elsevier.com/locate/jmr

Relationship between susceptibility induced field inhomogeneities, restricted diffusion, and relaxation in sedimentary rocks

Robert C. Wilson [a,*], Martin D. Hürlimann [b]

[a] Department of Bioengineering, University of Pennsylvania, Philadelphia, PA 19104, USA
[b] Schlumberger Doll Research, Ridgefield, CT 06877, USA

Received 9 May 2006; revised 2 July 2006
Available online 4 August 2006

Abstract

Low field relaxation and diffusion measurements have become essential tools to study the pore space of sedimentary rocks with important practical applications in the field of well logging and hydrocarbon extractions. Even at Larmor frequencies below 2 MHz, diffusion measurements are often affected noticeably by internal field inhomogeneities. These field inhomogeneities are induced by susceptibility contrast between the rock and the fluid and are evident in most sandstones. Using sets of two-dimensional diffusion–relaxation measurements in applied and internal gradients, we study in detail the correlation between the field inhomogeneities, restricted diffusion, and relaxation time in three rocks of different susceptibility. We find that in the sandstone cores, the field inhomogeneities in large pores can be described by a local gradient that scales inversely with relaxation time above 250 ms. At shorter relaxation times, the extracted internal gradients deviate from this scaling relationship and we observe a dependence on diffusion time. This demonstrates that in this case, the internal field has structure on a length scale of a few microns.

Keywords: Internal field; Susceptibility contrast; Diffusion–relaxation measurements; Porous media

1. Introduction

The geometrical characterization of the pore space of fluid filled porous media is an important problem in a range of different fields that includes chemical engineering, medicine, biology, soil science and the energy industry. A number of nuclear magnetic resonance techniques have been developed that rely on different aspects of the interactions between spins and the pore geometry.

Low field nuclear magnetic resonance has become an essential tool to study the pore space of sedimentary rocks with important practical applications in the field of well-logging and hydrocarbon extractions [1]. A widely used technique is the measurement of the distribution of relaxation times, T_2 [2]. Since relaxation in many rocks is dominated by surface relaxation, the T_2 distribution is often a reflection of the distribution of length scales that characterizes the pore space of rocks. A different approach is based on the measurement of the mean squared displacement of the fluid molecules undergoing Brownian motion [3]. Inside the pore space, diffusion is restricted by a degree that depends on the relative size of the pore opening and the diffusion length [4,5].

Two-dimensional diffusion–relaxation distribution functions [6] combine the strengths of the two methods. In this technique, the mean square displacement is measured along the direction of the applied gradient during a diffusion time T_d, $\langle (x(t_d) - x(0))^2 \rangle$, for each component of T_2, and it is compared to the expected displacement for unrestricted diffusion, $2D_0T_d$, for the appropriate molecular diffusion coefficient D_0. The degree of restriction can be expressed as normalized diffusion coefficient,

* Corresponding author.
E-mail address: rcwilson@seas.upenn.edu (R.C. Wilson).

1090-7807/$ - see front matter © 2006 Elsevier Inc. All rights reserved.
doi:10.1016/j.jmr.2006.07.006

$D(T_2)/D_0 \equiv \langle (x(t_d) - x(0))^2 \rangle / 2D_0 T_d$. For spins in porous media with uniform surface relaxation properties, the dependence of $D(T_2)/D_0$ on relaxation time is expected to be monotonic. Spins in large pores collide only infrequently with the walls, therefore the value of $D(T_2)/D_0$ approaches unity and the relaxation time is close to the bulk value of the fluid. In contrast, relaxation times of spins in small pores are much reduced from bulk values and $D(T_2)/D_0$ is reduced by the tortuosity of the pore space [7].

In the laboratory, diffusion measurements are generally performed using pulsed field gradients (PFG) [8,3]. In the application of well logging, it is more practical to take advantage of the existing static gradients of the logging tool [1] and it was demonstrated that this allows quantitative measurements of diffusion–relaxation distribution functions [6]. This implementation leads to slice selection effects that can be fully accounted for. However, in systems with significant susceptibility contrasts, the induced 'internal gradients' [9–12] can interfere with the applied gradient. Using static gradients, this effect cannot be suppressed as is commonly done using bipolar pulsed gradients [13,14]. Susceptibility effects are also greatly reduced by operating at low field strengths. Leu et al. [15] have compared the measurements of diffusion–relaxation distribution functions acquired in fixed gradient and with both uni- and bipolar pulsed gradients at a Larmor frequency of 2 MHz. Rocks with large susceptibility contrasts showed systematic differences.

The purpose of this paper is to study the restricted diffusion and susceptibility induced field inhomogeneities in sedimentary rocks and the correlation of these quantities with transverse relaxation times at low field. The degree of restriction [4,5], the susceptibility induced field inhomogeneities [16] and the relaxation rates [2] all contain an imprint of the local pore geometry and the strength of the internal gradient depends on the grain mineralogy [12,17]. A better understanding of these correlations will lead to an improved interpretation of diffusion measurements acquired in static gradients.

Sun and Dunn [18] have previously used a modified CPMG sequence to infer the correlation between internal field inhomogeneities and T_2 for two sandstones with varying amounts of paramagnetic impurities. They presented the results as distribution function of internal gradient and relaxation time. For each value of T_2, they found a wide distributions of internal gradients, but the average gradients tended to be higher for shorter values of T_2. This is consistent with the results presented here. Seland et al. [19] studied the correlation between internal gradients and transverse relaxation in samples of packed glass beads of different wettabilities and different saturation states.

To illustrate the degree of potential interference of internal gradients on the measurement of restricted diffusion, we present in Section 2 results on a large set of brine saturated rocks acquired in a static gradient at 1.76 MHz. Interference is apparent in most sandstones at short relaxation times. In Section 3, we review various implementations of the stimulated echo-CPMG pulse sequence with unipolar or bipolar pulsed gradients and discuss the different sensitivities to internal field gradients. Details of the experimental techniques are given in Section 4. In Section 5, we present measurements on three selected rocks, performed in a setup with uniform background field and pulsed field gradient (PFG) capability. Correlations between the strengths of the internal gradient and relaxation time are extracted. In addition, we discuss the spatial extents of the internal gradients.

2. Overview of D–T_2 measurements on brine saturated rocks in a static applied gradient

In Fig. 1, we show results of measurements of the normalized apparent diffusion coefficient versus relaxation time for 40 different rock cores saturated in brine. The experiments were performed in a static gradient of 13.2 G/cm and at an rf frequency of 1.764 MHz and used the stimulated echo-CPMG pulse sequence listed below in Fig. 2B. The diffusion time was fixed at $T_d = 20$ ms and the diffusion information was encoded by systematically changing the pulse spacings δ. Other experimental and processing parameters were identical to those given in [6].

The behavior of the D–T_2 measurements for the carbonate cores in Fig. 1 generally follows the expectations based on restricted diffusion. At long relaxation times, the typical pore openings are larger than $\sqrt{2D_0T_d} \approx 10$ μm and the reduction of $D(T_2)/D_0$ from unity is a monotonic function of relaxation time. At shorter relaxation times, the pore openings become smaller than $\sqrt{2D_0T_d}$ and the diffusion behavior is determined by the pore connectivity, or tortuosity. In this regime, the apparent diffusion coefficient is expected to become independent of relaxation time. This behavior is observed in many carbonate cores shown in Fig. 1. However, the majority of sandstones show a deviation from this behavior at short relaxation times with a pronounced upturn in the extracted value of the diffusion coefficient.

This behavior is consistent with the presence of sizeable 'internal gradients' in the smaller pores of sandstones. The susceptibility contrasts between grain and fluid in sandstones are generally higher than in carbonates [12] and can give rise to significant internal gradients even at the low applied magnetic fields used here [12,20,18]. Interference between internal and applied gradients leads to extra decay that is misinterpreted as an increased diffusion coefficient.

In principle, there are a number of alternate explanations for the anomalous behavior in sandstones. First, the intrinsic relaxation properties of the pore surfaces could be nonuniform due to heterogeneity in the mineralogical compositions of the grains. The relationship between restricted diffusion and relaxation is then not only a reflection of the pore space geometry, but also controlled by the heterogeneity of the grain mineralogy. In this model, the anomalous signal at short T_2 in

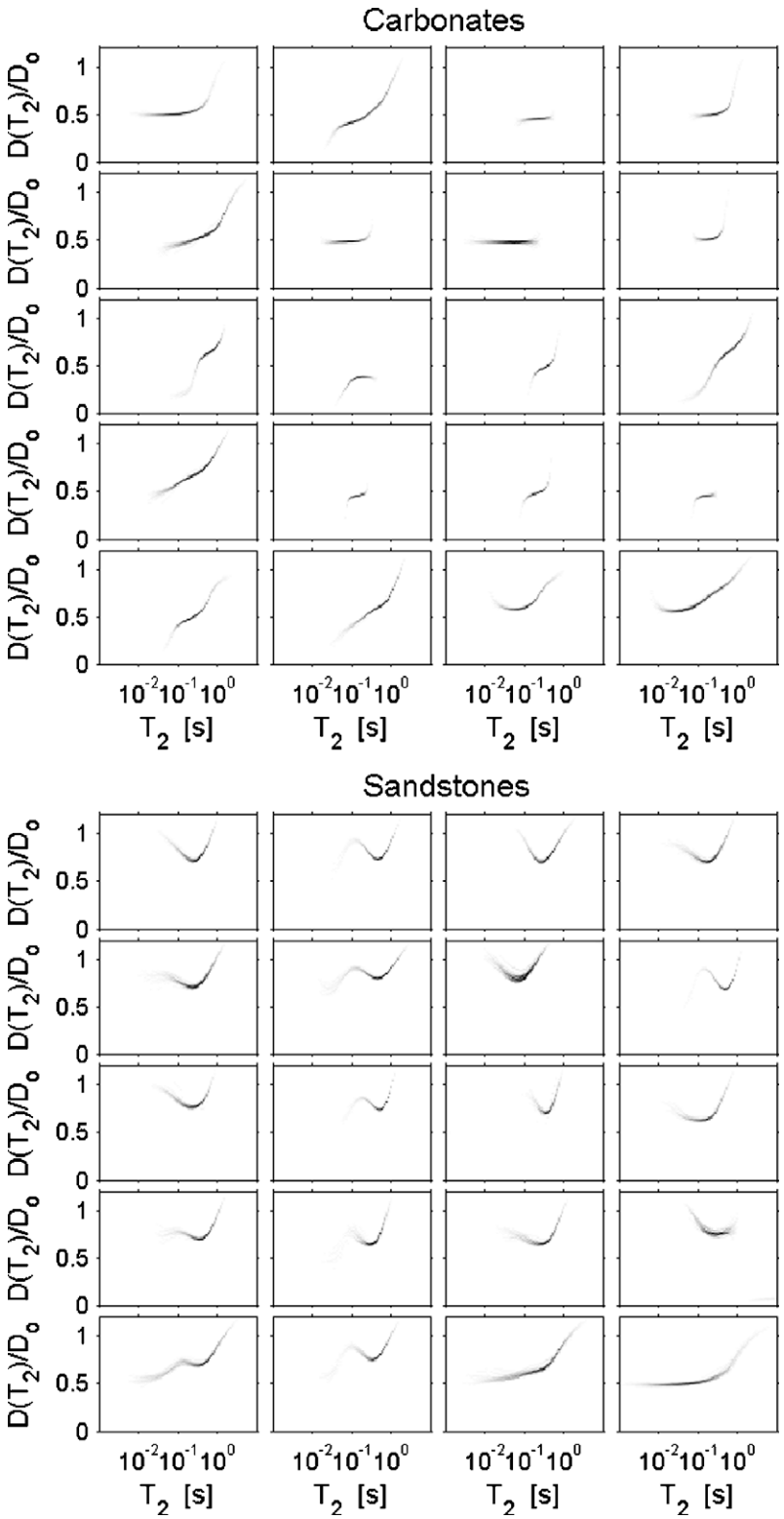

Fig. 1. Measured normalized apparent diffusion coefficient, $D(T_2)/D_0$, versus relaxation time, T_2, for 40 different cores of water saturated carbonate and sandstones samples. In all cases, the diffusion time T_d was set to 20 ms. The measurements were performed in the fringefield of a superconducting magnet at a Larmor frequency of 1.76 MHz and a static gradient of 13.2 G/cm with acquisition parameters and analysis procedures identical to those described in Ref. [6]. The carbonate cores show mostly the expected monotonic relationship between D and T_2, consistent with increasing restrictions at shorter T_2. However, most sandstones show a deviation from this behavior at short T_2. We show in this paper that this behavior is caused by susceptibility induced internal gradients.

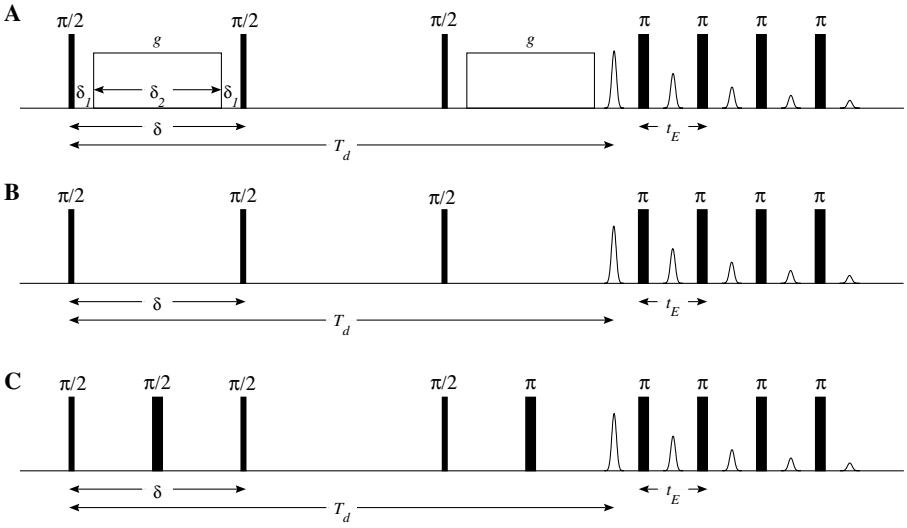

Fig. 2. Pulse sequences used to measure relationship between restricted diffusion, internal field inhomogeneities, and relaxation time T_2. (A) Stimulated echo sequence with pulsed field gradient, followed by a long train of closely spaced 180° pulses. (B) Identical sequence to (A) except for the absence of external field gradients. In this case, the spins are only exposed to the susceptibility induced internal field gradients. (C) Sequence with additional 180° pulses that refocus the magnetization during the diffusion encoding periods, δ. In our implementation, the diffusion time T_d and echo spacings t_E are fixed, but diffusion encoding times δ and δ_2 are varied systematically.

sandstones is due to spins in large pores with highly relaxing walls. A second possible explanation for the behavior is large (and uniform) surface relaxation. In this case, the magnetization decay is not in the fast diffusion limit [21] and the magnetization profile becomes inhomogeneous on a sub-pore length scale. The contributions associated with higher modes appear at short relaxation times and it was shown in [22] that these higher modes can exhibit very large apparent diffusion coefficients.

We have chosen three rocks with different susceptibility contrast to compare measurements performed in a uniform field with those using applied gradients. This allows us to demonstrate that the dominant mechanism for the observed anomalous behavior is associated with susceptibility induced gradients.

3. Theory for pulsed applied gradient

To investigate the presence of internal gradients and the degree of restricted diffusion, we performed a series of measurements using the pulse sequences shown in Fig. 2. Unlike the measurements shown in Fig. 1, these experiments were performed in a system with a uniform applied static field and pulsed gradient capability. All sequences consist of an initial diffusion encoding sequence, followed by a CPMG-like sequence [23–25].

The sequence shown in Fig. 2A was first used by Peled et al. [25]. In their application, the diffusion information was obtained by changing the gradient strength g systematically. Here in analogy to the constant gradient application, we fix the strength of g and change the duration δ_2. In anticipation to the study of internal gradients, we have also included in Fig. 2B and C two sequences, where the applied gradient is set to zero and the measurement is only affected by the internal gradients. In Fig. 2C, extra π pulses refocus the magnetization during the encoding time δ and attenuate the effect of internal gradients. This sequence corresponds to the well-known bipolar gradient sequence of Cotts et al. [13] with zero applied strength. As will be discussed below, a comparison of results obtained with sequences B and C can be used to obtain information about the correlation length of internal gradients.

3.1. Measuring D–T_2 distribution functions in the absence of internal gradients

In the absence of internal gradients, the magnetization of the echoes can be written as

$$M(g\delta_1, kt_E) = \int\int\int \mathrm{d}D\,\mathrm{d}T_2\,\mathrm{d}T_1 f(D,T_2,T_1) k_1(D,g\delta_1,T_1,T_2) k_2(T_2,kt_E). \tag{1}$$

Here, $k_1(D,g\delta_1,T_1,T_2)$ is the diffusion kernel for the first part of the sequence, $k_2(T_2,kt_E)$ is the relaxation kernel for the CPMG-like second part of the sequence, and $f(D,T_2,T_1)$ is the distribution function that characterizes the relationship between diffusion coefficient, D, and the relaxation times T_1 and T_2. This distribution function contains the structural information on the pore geometry of the rock [6]. The relaxation kernel for the k-th echo with echo spacing of t_E is given by

$$k_2(T_2, kt_E) = \exp\left\{-\frac{kt_E}{T_2}\right\}. \tag{2}$$

For the first sequence in Fig. 2, the kernel k_1 is given by:

$$k_1(D, g\delta_1, T_1, T_2) = \frac{1}{2} \times \exp\left\{-\gamma^2 g^2 \delta_2^2 D\left(T_d - \frac{4}{3}\delta_2 - 2\delta_1\right)\right\} \times \exp\left\{-\frac{T_d}{T_1} - 2\delta\left(\frac{1}{T_2} - \frac{1}{T_1}\right)\right\}. \quad (3)$$

It is useful to introduce $f_{T_d}(D, T_2)$ defined as

$$f_{T_d}(D, T_2) \equiv \int dT_1 f(D, T_2, T_1) \exp\left\{-\frac{T_d}{T_1}\right\}. \quad (4)$$

It can be interpreted as the diffusion relaxation distribution function of spins surviving at a diffusion time T_d. Next, for small δ, $\exp\{-2\delta(\frac{1}{T_2} - \frac{1}{T_1})\} \approx 1$ and we can write Eq. (1) in a form with a separable kernel with respect to D and T_2.

$$M(\delta, kt_E) \approx \frac{1}{2}\int\int dD\, dT_2 f_{T_d}(D, T_2) \times \exp\left\{-\gamma^2 g^2 \delta_2^2 D\left(T_d - \frac{4}{3}\delta_2 - 2\delta_1\right)\right\} \exp\left\{-\frac{kt_E}{T_2}\right\}. \quad (5)$$

In other words, $M(\delta,kt_E)$ is related to the two-dimensional Laplace transform of $f_{T_d}(D, T_2)$. This distribution function can therefore be obtained from the measured magnetization by using an inversion scheme such as [26].

In our application, the measured diffusion coefficient D is reduced from the molecular diffusion coefficient D_0 due to restrictions imposed by the local geometry of the pore space. In this case, Eq. (5) becomes an approximation. For strong diffusion effects, restrictions will lead to deviations from the Gaussian phase distribution and modify the exact diffusion dependence in Eq. (5) at low signal levels. This complication can obscure some details in $f_{T_d}(D, T_2)$. At small attenuation, however, Eq. (5) remains correct, which implies that the first moment $D(T_2) \equiv \int dD D f_{T_d}(D, T_2) / \int dD f_{T_d}(D, T_2)$ is a robust quantity and unaffected by these effects. For this reason, we concentrate below on $D(T_2)$ rather than the full extracted D–T_2 distribution functions.

3.2. Interference by internal field gradients

The presence of susceptibility induced field inhomogeneities complicates the situation. These inhomogeneities have in general a complicated spatial dependence as they carry the imprint of the pore geometry [16]. If the diffusion length $\sqrt{DT_d}$ is much shorter than the pore size, we can approximate the field inhomogeneity experienced by a spin by a local internal gradient $\mathbf{g}_b$.

Tanner [27] showed that the attenuation due to free diffusion in the case of the monopolar sequence with applied gradient $\mathbf{g}_a$, and static and spatially uniform background gradient $\mathbf{g}_b$ can be written as

$$k_1 = \exp\left\{-\gamma^2 D\left[C_a g_a^2 + C_b g_b^2 + C_{ab}\mathbf{g}_a \cdot \mathbf{g}_b\right]\right\} \quad (6)$$

where $g_a = |\mathbf{g}_a|$, $g_b = |\mathbf{g}_b|$ and the coefficients C_a, C_b and C_{ab} are given by

$$\begin{aligned} C_a &= \delta_2^2\left(T_d - \tfrac{4}{3}\delta_2 - 2\delta_1\right), \\ C_b &= \delta^2\left(T_d - \tfrac{4}{3}\delta\right), \\ C_{ab} &= -2\delta\left(\delta T_d - \delta^2 - \tfrac{1}{3}\delta_2^2 - \delta_1\delta_2 - \delta_1^2\right). \end{aligned} \quad (7)$$

In the case of porous media, the susceptibility induced gradients span a range of values that vary in a non-trivial manner with the local structure of the pore geometry. To first order, we expect that the strength of the local gradient scales inversely with the local pore opening. Since the relaxation time T_2 scales also with pore size, we expect that the relaxation time and local gradient experienced by spins show a strong correlation. To proceed we consider the fraction, $P(\mathbf{g}_b,T_2)$, of spins in the rock experiencing a particular background gradient $\mathbf{g}_b$ and relaxing with relaxation time T_2. We further make the assumption that the background gradients are spatially uniform on a length scale $\sqrt{DT_d}$, such that the Tanner formula, Eq. (6), is applicable to each subset. Finally, we make the assumption that these subsets are independent and that each subset diffuses with diffusion constant $D(T_2)$. Therefore, we can write the signal as the volume average of all of the subsets, i.e.

$$k_1 = \int d\mathbf{g}_b P(\mathbf{g}_b, T_2) \times \exp\left\{-\gamma^2 D(T_2)\left[C_a g_a^2 + C_b g_b^2 + C_{ab}\mathbf{g}_a \cdot \mathbf{g}_b\right]\right\}. \quad (8)$$

For sufficiently small internal gradients such that $\gamma^2 D C_{ab}\mathbf{g}_a \cdot \mathbf{g}_b \ll 1$ and $\gamma^2 D C_b g_b^2 \ll 1$ we can write

$$\begin{aligned} k_1 &\approx \exp\left\{-\gamma^2 D(T_2)\left[C_a g_a^2 + C_b \int d\mathbf{g}_b P(\mathbf{g}_b, T_2) g_b^2 + C_{ab}\int d\mathbf{g}_b P(\mathbf{g}_b, T_2)\mathbf{g}_a \cdot \mathbf{g}_b\right]\right\} \\ &\approx \exp\left\{-\gamma^2 D(T_2)\left[C_a g_a^2 + C_b\langle g_b^2(T_2)\rangle\right]\right\} \\ &= \exp\left\{-\gamma^2 D(T_2)\left[1 + \frac{C_b\langle g_b^2(T_2)\rangle}{C_a g_a^2}\right] C_a g_a^2\right\} \\ &= \exp\left\{-\gamma^2 D_A(T_2) C_a g_a^2\right\}. \end{aligned} \quad (9)$$

Here, we have written $\langle g_b^2(T_2)\rangle = \int P(\mathbf{g}_b, T_2) g_b^2 d\mathbf{g}_b$ as the mean square background gradient for spins with a given relaxation time T_2 and we have taken advantage of the fact that $\int P(\mathbf{g}_b, T_2)\mathbf{g}_b d\mathbf{g}_b = 0$ in a random media. We have also introduced the apparent diffusion coefficient for sequence A, $D_A(T_2)$:

$$D_A(T_2) = D(T_2)\left[1 + \frac{C_b}{C_a}\frac{\langle g_b^2(T_2)\rangle}{g_a^2}\right]. \quad (10)$$

The apparent diffusion coefficient has a simple interpretation. If diffusion data is acquired by varying the length of the gradient pulses, δ_1, and is analyzed using Eq. (3), which assumes that there are no background gradients, the extracted diffusion coefficient corresponds to $D_A(T_2)$ rather than the desired $D(T_2)$.

The net T_2 dependence of the apparent diffusion coefficient $D_A(T_2)$ is the result of two opposing effects: the effect of restricted diffusion, characterized by $D(T_2)$, generally decreases the diffusion coefficient with decreasing T_2, whereas the effect of internal gradients, characterized by $\langle g_b^2(T_2)\rangle$, increases the apparent diffusion coefficient with decreasing T_2.

In the presence of sufficiently large internal gradients, the cross term between g_a and g_b can no longer be ignored and the small gradient assumption made in the derivation of Eq. (9) will break down. As shown in [13,14], the apparent diffusion coefficient extracted from kernel k_1 without this cross term underestimates the true diffusion coefficient in this case. In the context of this work, it is fairly straightforward to show that the attenuation due to kernel k_1 as expressed in Eq. (8) is less than the attenuation due to k_1 expressed in Eq. (9), consistent with a smaller measured diffusion coefficient, i.e.

$$\int d\mathbf{g}_b P(\mathbf{g}_b, T_2) \exp\left\{-\gamma^2 D(T_2)\left[C_a g_a^2 + C_b g_b^2 + C_{ab}\mathbf{g}_a\cdot\mathbf{g}_b\right]\right\} > \exp\left\{-\gamma^2 D_A(T_2) C_a g_a^2\right\}. \quad (11)$$

3.3. Measurements without external field gradient

The interference between applied and internal gradient is usually mitigated by changing systematically the strength of the applied gradient g_a rather than its duration and by using the bipolar gradient sequence by Cotts et al. [13]. The goal of the present study is to characterize internal gradients, rather than suppressing them. For this purpose, we have used sequence B in Fig. 2 without applied gradient.

The signal for sequence B has the same form as Eq. (5), except we set $\delta_1 = 0$, $\delta_2 = \delta$, and we interpret g as the internal gradient g_b. To analyze the results of this sequence, it is useful to express the internal gradients in terms of the apparent diffusion coefficient D_B by fitting the δ dependence to the diffusion kernel $\exp\{-\gamma^2 C_a D_B g_{ref}^2\}$, where the reference gradient g_{ref} is conveniently chosen to be equal to strength of applied gradient in the other experiments, g_a.

By setting $g_a = 0$ in Eq. (9), the apparent diffusion coefficient $D_B(T_2)$ is then proportional to the mean squared internal gradient, $\langle g_b^2(T_2)\rangle$ and is given by:

$$D_B(T_2) = D(T_2)\frac{C_b}{C_a}\frac{\langle g_b^2(T_2)\rangle}{g_{ref}^2}. \quad (12)$$

Note that since $D(T_2) \leqslant D_0$ and in practice $C_b/C_a \approx 1$ (as $\delta_2 \ll \delta_1$) then the normalized apparent diffusion coefficient $D_B(T_2)/D_0$ is effectively a lower limit on $\langle g_b^2(T_2)\rangle$ in units of g_{ref}^2.

The relevant internal gradient for spins diffusing in porous media such as sedimentary rocks is an average over the diffusion time T_d. The analysis above implicitly assumes that the internal gradient is spatially uniform over the typical diffusion length of the spins, $\sqrt{DT_d}$. To test this assumption, measurements with different diffusion time T_d were performed. A dependence of the extracted values of $\langle g_b^2(T_2)\rangle$ on T_d will indicate that the local internal gradients are not uniform on the length scale of $\sqrt{DT_d}$, which is typically of the order of 10 μm. To probe structure on a shorter length scale, we have also performed measurements with the sequence shown in Fig. 2C. In the case of a static uniform background gradient g_b, the additional π pulses refocuses the magnetization and greatly reduces the diffusion sensitivity. For a static, uniform background gradient g_b, the diffusion kernel for sequence B, $\exp\{-\gamma^2 g_b^2 D\delta^2(T_d - 4/3\delta)\}$, becomes $\exp\{-\gamma^2 g_b^2 D\delta^2(\delta/6)\}$ for sequence C. We can interpret this as a reduction of the effective diffusion time $T_d - 4/3\delta$ in sequence B to the much shorter time $\delta/6$, i.e.

$$D_C \simeq \frac{\frac{1}{6}\frac{\delta}{T_d}}{1-\frac{4}{3}\frac{\delta}{T_d}} D_B. \quad (13)$$

4. Experimental

To probe the full range of effects we present results from four different samples: a bulk fluid sample that does not exhibit internal gradients or restrictions, and three brine saturated cores of sedimentary rock with different susceptibility contrasts. For the bulk fluid sample, we used water, doped with $NiCl_2$ to reduce the relaxation time to a value similar to those in rocks. The three rock cores were Indiana limestone, Berea sandstone, and a chlorite rich sandstone. Indiana limestone is characterized by a wide range of pore sizes, has a porosity of 0.15, a permeability of 0.006 μm^2 and a low susceptibility contrast to water, $\Delta\chi = 3.0\times10^{-6}$ (in SI units). Berea is a sandstone with moderate clay content, a porosity of 0.175, permeability of 0.17 μm^2 and a susceptibility contrast of $\Delta\chi = 9.9\times10^{-5}$. The chlorite rich sandstone has a porosity of 0.23, a permeability of 0.39 μm^2 and a susceptibility contrast of $\Delta\chi = 2.8\times10^{-4}$. Chlorite is a pore lining clay and is therefore especially efficient at producing internal field inhomogeneities in the pore space [20]. This core represents an extreme case where susceptibility induced gradients can be expected to be comparable to, or even dominate the applied gradient, even at low field and in large pores.

We performed the same experiments on all four samples, using the pulse sequences of Fig. 2. All experiments were performed on a MARAN Ultra benchtop spectrometer running at a ^1H Larmor frequency of 2 MHz. The durations of the 90° and 180° pulses were typically 15.5 and 31 μs, respectively. Measurements were performed at $T = 30$ °C. In the diffusion editing part of each pulse sequence, the diffusion time T_d was set first to 20 and then 50 ms. In sequence A, the amplitude of the external gradient was set to 14.1 G/cm, comparable to that in previous fringe field measurements [6]. Five values of δ were chosen in such a way that the logarithm of the kernel k_1 was

sampled uniformly, i.e. $\gamma^2 g^2 D_0 \delta^2 (T_d - \frac{4}{3}\delta)$ was set to 0, 0.25, 0.5, 0.75, and 1. Here, D_0 is the molecular diffusion coefficient of water. For the CPMG-like part of each pulse sequence, we acquired 4096 echoes with an echo spacing of $t_E = 375.2$ μs.

5. Results

Fig. 3 gives an overview of the measured amplitudes for $T_d = 20$ ms. In each panel, the five lines represent the measured echo amplitudes for five different values of δ. The separation between the lines is caused by diffusion. The main effects of interest are readily evident in the raw data.

The water sample shows the expected behavior for unrestricted diffusion in the absence of internal field inhomogeneities. The applied gradient of sequence A results in diffusion induced separation of the curves, whereas for sequence B and C without external gradients, the five curves fall on top of each other. In the Indiana limestone sample, the diffusion encoding of sequence A generates a smaller separation of the five curves. This is caused by restricted diffusion that effectively lowers the relevant diffusion coefficient. Since the five curves essentially collapse for sequence B and C, we conclude that the internal gradients in Indiana limestone are small. In the chlorite rich sandstone, the initial separation between the curves for sequence A is larger than for water. This suggests that in this case, the internal gradients are significant and have to be of magnitude comparable to the applied gradient. This is confirmed by the results for the sequence without applied gradients, shown in the second column, that show a pronounced separation. The third column displays the results from sequence C that includes a 180° refocusing pulse in the diffusion encoding intervals. As with pulse sequence B, the water and Indiana limestone CPMG trains collapse on a single line while those of the Berea and the chlorite rich sandstone samples do not. However the spread in the latter two is diminished in comparison to the monopolar experiment (sequence B). This indicates that the effects of the background gradients are partially, but not completely refocused.

5.1. Correlation of internal gradient with relaxation

For a more quantitative analysis, we study the correlation of the diffusion effects with relaxation. In Fig. 4, we

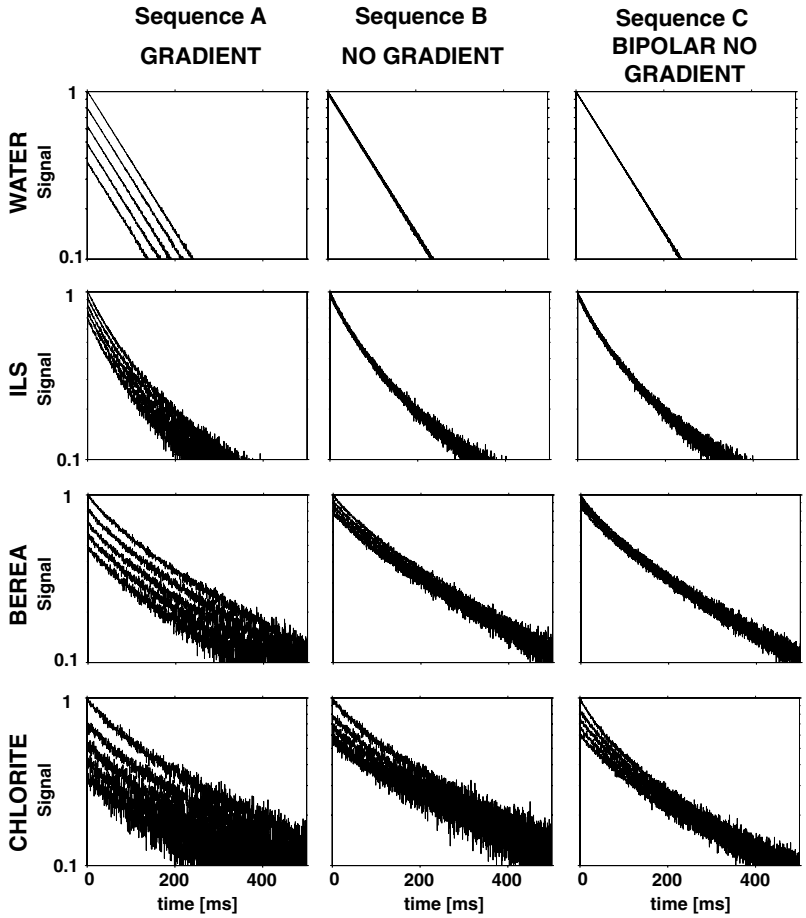

Fig. 3. Each row shows the measured echo amplitudes versus echo time for the three sequences shown in Fig. 2, using $T_d = 20$ ms. Each plot shows five CPMG decays for different values of δ. Each row represents results from different samples (water, Indiana limestone, Berea sandstone and a chlorite rich sandstone).

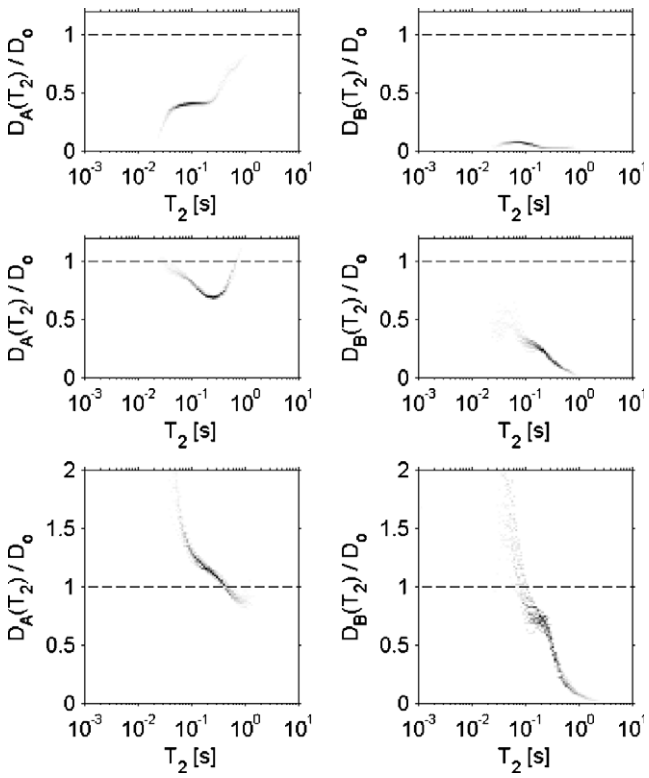

Fig. 4. Measurement of effective diffusion coefficients D_A (left) and D_B (right) versus relaxation time T_2 for the three samples, Indiana limestone (top row), Berea sandstone (middle row) and the chlorite rich sandstone sample (bottom row). As explained in the text, D_A was measured with sequence A using external pulsed gradient of 14.1 G/cm, whereas D_B was measured with sequence B without external gradient. The diffusion time was $T_d = 20$ ms.

present results for sequences A and B on the three rock cores. As discussed above in Section 3, we use the kernels $k_1 = \exp\{-\gamma^2 C_a g_{ref}^2 D\}$ and $k_2 = \exp\{-kt_E/T_2\}$ to extract the diffusion–relaxation distribution function $f_{T_d}(D, T_2)$ by a two-dimensional Laplace inversion. In Fig. 4, we plot the average apparent diffusion coefficient $D_i(T_2) \equiv \int dD D f_{T_d}(D, T_2) / \int dD f_{T_d}(D, T_2)$ versus T_2. Here, $i = A$ or B indicates the sequence used. The intensity of the curves is proportional to $\int dD f_{T_d}(D, T_2)$. Following the procedure in [6], we tested the stability of the inversion by generating 40 reconstructed data sets with different noise realizations from the fits. The results in Fig. 4 are a superposition of all the inversion results; the widths of the curves therefore give some indication of the uncertainties of the inversion.

The results of $D_A(T_2)$ for the three samples show the full range of responses. Indiana limestone displays a small monotonic increase of $D_A(T_2)$ with T_2, consistent with restricted diffusion and wall relaxation. In this case, $D_A(T_2)$ is dominated by the first term in Eq. (10). In contrast, the results for the chlorite rich sandstone show a decrease of $D_A(T_2)$ with T_2. For a large range of T_2, the extracted diffusion coefficient D_A is larger than the molecular diffusion coefficient, D_0. This is an indication that $D_A(T_2)$ for this rock is controlled by internal gradients and that the second term dominates in Eq. (10). The results for Berea sandstone show an intermediate case where the T_2 dependence of D_A is non-monotonic. At short T_2, the second term in Eq. (10) dominates, while at long T_2 the first term dominates.

This interpretation is confirmed by the results of D_B shown on the right hand side in Fig. 4. Indiana limestone shows small values of D_B, reflecting the near collapse of the raw data in Fig. 3. In contrast, D_B for Berea and chlorite rich sandstone samples are clearly non-zero, which indicates significant background gradients. This proves that the upturn of D_A at short T_2 shown on the left hand side of Fig. 4 is caused by internal gradients and rules out the other possible effects considered earlier.

From the measurements of D_A and D_B, it is possible to extract the 'internal gradient free' diffusion coefficient $D(T_2)$, that is directly related to the mean squared displacement, and the mean squared internal gradient, $\langle g_b^2(T_2)\rangle$. In the framework of our theoretical analysis and setting $g_{ref} = g_a$, we obtain from Eqs. (10) and (12).

$$D(T_2) = D_A(T_2) - D_B(T_2). \tag{14}$$

$$\frac{\langle g_b^2(T_2)\rangle}{g_{ref}^2} = \frac{C_a}{C_b}\frac{D_B(T_2)}{D_A(T_2) - D_B(T_2)}. \tag{15}$$

The results of $D(T_2)$ and $\sqrt{\langle g_b^2(T_2)\rangle}$ for the three rocks are shown in Fig. 5. The results show a number of general features that support our approach. First, the extracted diffusion coefficient $D(T_2)$ are now bound by the molecular diffusion coefficient, D_0, even for the chlorite rich sandstone where $D_A(T_2)$ is generally significantly larger than D_0. In addition, the upturn of the diffusion coefficient at short T_2 in the Berea and chlorite rich sandstone is greatly reduced in $D(T_2)$ compared to $D_A(T_2)$. This confirms that the observed non-monotonic behavior of the diffusion coefficient D_A versus T_2 is mainly caused by internal field inhomogeneities and can be modelled to first order with our approach.

The results on the internal gradients in Fig. 5 quantify some of our earlier observations: the magnitude of $\sqrt{\langle g_b^2(T_2)\rangle}$ in Indiana limestone is substantially smaller than the applied gradient g_a, in Berea sandstone the magnitudes become comparable to g_a at shorter T_2, and in the chlorite rich sandstone, $\sqrt{\langle g_b^2(T_2)\rangle}$ exceeds g_a at relaxation times below 300 ms. For each rock, the internal gradients decrease with increasing T_2.

5.2. Spatial extent of internal gradients

For T_2 values above 250 ms, we observe that the magnitude of the internal gradient is inversely proportional to T_2. This is consistent with the simplest model for relaxation and internal field inhomogeneities. In sufficiently large pores, the pore size l_s is larger than the typical range that spins explore during the encoding time, $\sqrt{D_0 T_d}$. The field inhomogeneities experienced by a spin during the diffusion encoding interval can then be approximated reasonably

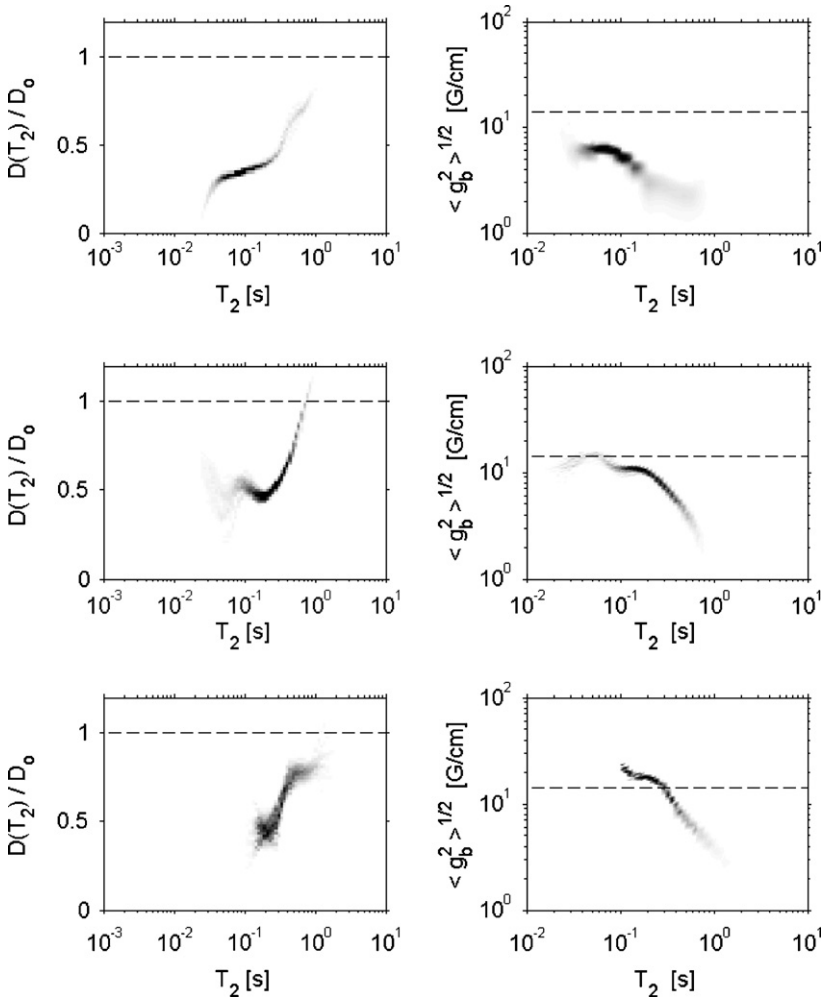

Fig. 5. Plots of restricted diffusion coefficient, $D(T_2)/D_0$, corrected for susceptibility effects versus T_2 (left) and average internal gradient, $\sqrt{\langle g_b^2(T_2)\rangle}$, versus T_2 (right) for the three different samples, Indiana limestone (top row), Berea sandstone (middle row) and the chlorite rich sandstone sample (bottom row). The dashed line on the left panels indicates unrestricted diffusion, $D(T_2) = D_0$. On the right, the dashed line indicates the value of the external gradient used in the experiments with sequence A, $g = 14.1$ G/cm.

well by a gradient, g_b. In the whole pore, the gradients have a wide distribution, consistent with the results of Sun and Dunn [18]. In our experiments, we are measuring the average of $\langle g_b^2\rangle$ for spins having a particular value of T_2. To first order, we expect that the relaxation time is proportional to pore size, l_s, whereas the average internal gradient is inversely proportional to the pore size. This leads to the observed scaling between $\sqrt{\langle g_b^2(T_2)\rangle}$ and T_2. The identification of this regime as large pore regime is further supported by the diffusion results. In this regime, we find $D(T_2)/D_0 > 0.5$, i.e. diffusion is only moderately restricted, consistent with large pores.

At shorter values of T_2, we observe a slower dependence of $\sqrt{\langle g_b^2(T_2)\rangle}$ on T_2. Several effects can contribute to this deviation.

First we only expect an inverse linear relationship if the relaxation and gradient are controlled by the same geometrical length scales. As an extreme example consider a rock with grains of varying susceptibility but uniform surface relaxivity. In such a system, the relaxation rates are determined by the pore sizes, but the gradients are controlled predominantly by the size of the most magnetic grains. Furthermore, in pores comparable to or smaller than the diffusion length $\sqrt{D_0 T_d}$, the field inhomogeneities experienced by a spin during the diffusion encoding interval cannot be approximated anymore by a uniform gradient. In sufficiently small pores, diffusion effectively averages out the field inhomogeneities experienced by the spins. When the average traversal rate across the pore, D/l_s^2, is higher than the spread in Larmor frequencies across the pore, typically $\Delta\chi B_0$ [9], then the spins effectively average out the field inhomogeneities [28]. In this situation, we measure effective gradients that are much smaller than the microscopic gradient of the local magnetic field [12]. Song et al. [16] have used this effect to estimate pore size distributions by measuring the times needed for spins to diffuse a distance for the local field to become uncorrelated with that at the initial position.

Finally, as mentioned above, the small gradient approximation used in the derivation of Eq. (9) becomes

inaccurate at higher gradients. In our experiments, this problem starts to become noticeable when the effective gradients exceed 10 G/cm. This effect will tend to underestimate the true gradient.

Following the approach of Song et al. [16], we can probe the spatial extent of the internal gradients by varying the diffusion time T_d. Fig. 6 compares results obtained for $T_d = 20$ and 50 ms that correspond to length scales of $\sqrt{DT_d}$=7 and 11 μm. The measurements of $\sqrt{\langle g_b^2(T_2)\rangle}$ for Berea sandstone show that in the 'linear range' above T_2 of 250 ms, the extracted gradients are independent of T_d. This implies that the corresponding pore sizes are larger than 11 μm. At shorter T_2, the internal gradients at 50 ms now shows a slight downturn that is consistent with increased diffusive averaging.

Structure of the local field inhomogeneities on a shorter length scale can be probed with the modified pulse sequence shown in Fig. 2C that includes extra refocusing pulses in the diffusion encoding intervals. The sequence is identical to the well-known sequence of Cotts et al. [13] without the applied bipolar gradients. The degree of suppression of the diffusion effect by the refocusing pulses depends on the profile of the internal field. For fields that can be characterized by a uniform gradient over a length scale $\sqrt{DT_d}$, the extra 180° pulses refocus most of the phase acquired by the spins during the intervals δ. This greatly reduces the diffusion sensitivity and the extracted diffusion coefficient D_C is much smaller than D_B, and given by Eq. (13). In the other limiting case where the field has large fluctuations and is uncorrelated over a length scale of $\sqrt{D\delta}$, the extra 180° pulses will have little effect and the two pulse sequences of Fig. 2B and C will give similar results with $D_C \simeq D_B$.

The results for D_B and D_C for Berea sandstone are shown in Fig. 7. The values for D_C are lower than D_B, which indicates that the extra 180° refocusses the magnetization at least partially. For $T_d = 20$ ms shown on top, the maximum value of $\delta/T_d = 0.24$, while for $T_d = 50$ ms, the corresponding ratio is $\delta/T_d = 0.05$. Based on Eq. (13), the expected ratio of D_C/D_B for uniform gradients is then 0.06 and 0.009, respectively. It is apparent that the measured values of D_C shown in Fig. 7 are significantly higher than these

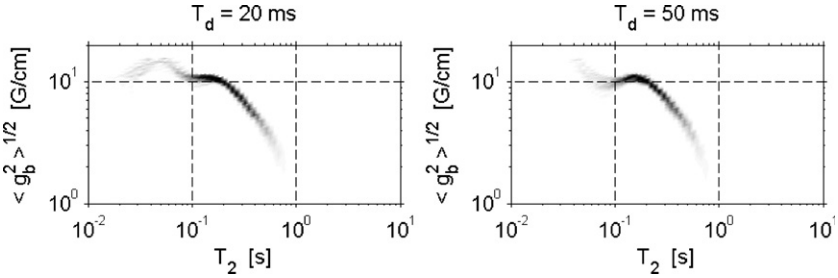

Fig. 6. Internal gradient versus T_2 for the Berea sandstone, measured at two different diffusion times T_d: 20 ms (left) and 50 ms (right).

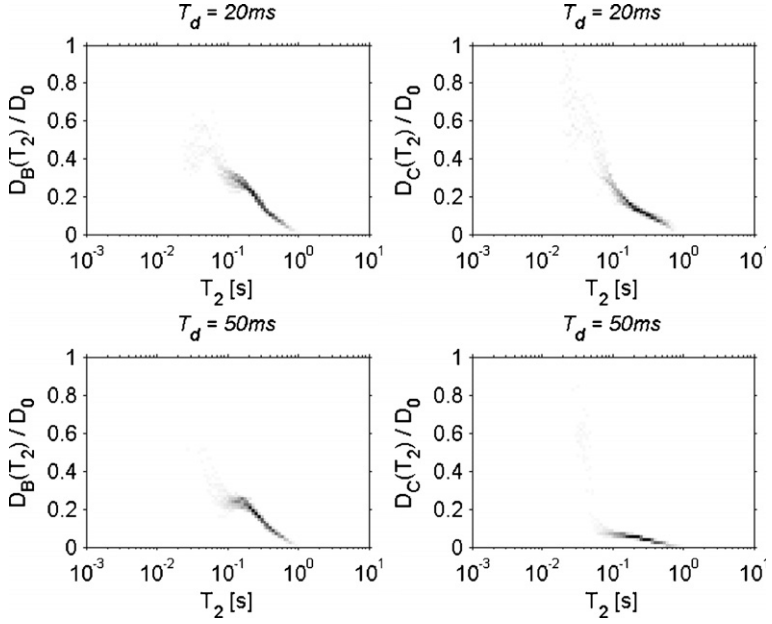

Fig. 7. Effect of extra refocusing pulses in diffusion encoding interval on extracted diffusion coefficient versus T_2 for Berea sandstone. The left panels show D_B versus T_2 measured with sequence B, while the right panels show D_C measured with sequence C. The top panels are results for $T_d = 20$ ms, the bottom panels for $T_d = 50$ ms. Although the 180° pulses reduce the effects of the background gradients and lead to $D_C < D_B$, the reduction is less than expected from Eq. (13). This suggests that g_b varies on a length scale comparable to $\sqrt{D\delta}$.

predictions. This implies that the spatial dependence of the internal field is more complicated than a simple gradient and must have some structure on a micron level.

Such rapid field variations likely occur close to the pore walls. Brown and Fantazzini have pointed out that sharp corners on grain surfaces can generate divergent susceptibility induced magnetic fields [9,29]. In addition, the susceptibility of sandstones with mixed mineralogy is not uniform. Clay minerals, such as pore lining chlorite, can generate large local gradients [30,17]. In such cases, the structure of the internal field is not only controlled by the pore opening, but also by the dimensions of clay flakes.

6. Conclusion

We have investigated experimentally the relationship between susceptibility induced field inhomogeneities, restricted diffusion and relaxation in three rock cores. We demonstrate that even at the low Larmor frequency of 2 MHz, the internal gradients can be large enough to interfere with restricted diffusion measurements, especially in sandstones at short relaxation times, T_2. However, with the short echo spacing used in the experiments, the gradients are not high enough to affect the T_2 measurements significantly.

It is remarkable that the presence of the upturn of D_A at short T_2 can be used as a good indicator to distinguish sandstones from carbonate rocks. The last two samples of carbonates in Fig. 1 have unusually high susceptibilities for carbonates, whereas the last two samples of sandstones have unusually low susceptibilities for sandstones.

We show that a simple model can account for the main effects. By combining measurements performed with and without an applied gradient, we can extract a restricted diffusion coefficient versus T_2 that is to first order corrected for the susceptibility effect. It also allows us to estimate the average internal gradient $\sqrt{\langle g_b^2 \rangle}$ as a function of relaxation time. We show that for T_2 longer than 250 ms, the data is consistent with a large pore regime. In this regime, the field inhomogeneity over 10 μm can be described by a gradient that is inversely proportional to the relaxation time. However, we find clear evidence that over the micron level, the internal field has additional structure that is likely associated with clay minerals or sharp corners of the grains.

At shorter relaxation times, the extracted average gradient depends on the diffusion time and shows a weaker dependence on the relaxation rate. In this case, the pores are smaller than the diffusion length $\sqrt{DT_d}$ and the constant gradient picture fails.

References

[1] R.L. Kleinberg, Encyclopedia of Nuclear Magnetic Resonance, Chapter Well logging, vol. 8, John Wiley, Chichester, 1996, pp. 4960–4969.

[2] W.E. Kenyon, Nuclear magnetic resonance as a petrophysical measurement, Nucl. Geophys. 6 (1992) 153.

[3] P.T. Callaghan, Principles of Nuclear Magnetic Resonance Microscopy, Clarendon Press, Oxford, 1991.

[4] D.E. Woessner, NMR spin-echo self-diffusion measurements on fluids undergoing restricted diffusion, J. Phys. Chem. 67 (1963) 1365–1367.

[5] P.P. Mitra, P.N. Sen, L.M. Schwartz, P. Le Doussal, Diffusion propagator as a probe of the structure of porous media, Phys. Rev. Lett. 68 (1992) 3555–3558.

[6] M.D. Hürlimann, L. Venkataramanan, Quantitative measurement of two dimensional distribution functions of diffusion and relaxation in grossly inhomogeneous fields, J. Magn. Reson. 157 (2002) 31–42.

[7] M.D. Hürlimann, K.G. Helmer, L.L. Latour, C.H. Sotak, Restricted diffusion in sedimentary rocks: determination of surface-area to volume ratio and surface relaxivity, J. Magn. Reson. A 111 (1994) 169–178.

[8] E.O. Stejskal, J.E. Tanner, Spin diffusion measurements: spin echoes in the presence of a time-dependent field gradient, J. Chem. Phys. 42 (1965) 288–292.

[9] R.J.S. Brown, P. Fantazzini, Conditions for initial quasilinear T_2^{-1} versus τ for Carr–Purcell–Meiboom–Gill NMR with diffusion and susceptibility differences in porous media and tissues, Phys. Rev. B 47 (1993) 14823.

[10] R.L. Kleinberg, M.A. Horsfield, Transverse relaxation processes in porous sedimentary rock, J. Magn. Reson. 88 (1990) 9.

[11] L.L. Latour, L. Li, C.H. Sotak, Improved PFG stimulated-echo method for the measurement of diffusion in inhomogeneous fields, J. Magn. Reson. B 101 (1993) 72.

[12] M.D. Hürlimann, Effective gradients in porous media due to susceptibility differences, J. Magn. Reson. 131 (1998) 232–240.

[13] R.M. Cotts, M.J.R. Hoch, T. Sun, J.T. Markert, Pulsed field gradient stimulated echo methods for improved NMR diffusion measurements in heterogeneous systems, J. Magn. Reson. 83 (1989) 252–266.

[14] P.Z. Sun, J.G. Seland, D. Cory, Background gradient suppression in pulsed gradient stimulated echo measurements, J. Magn. Reson. 161 (2003) 168–173.

[15] G. Leu, E.J. Fordham, M.D. Hürlimann, P. Frulla, Fixed and pulsed gradient diffusion methods in low field core analysis, Magn. Reson. Imaging 23 (2005) 305–309.

[16] Y. Song, S. Ryu, P.N. Sen, Determining multiple length scales in rocks, Nature 406 (2000) 178–181.

[17] M.D. Hürlimann, A. Matteson, J.E. Massey, D.F. Allen, E.J. Fordham, F. Antonsen, H.G. Rueslåtten, Application of NMR diffusion editing as chlorite indicator, Petrophysics 45 (2004) 414–421.

[18] B. Sun, K. Dunn, Probing the internal field gradient of porous media, Phys. Rev. E 65 (2002) 051309.

[19] J.G. Seland, K.E. Washburn, H.W. Anthonsen, J. Krane, Correlations between diffusion, internal magnetic field gradients, and transverse relaxation in porous systems containing oil and water, Phys. Rev. E 70 (2004) 51305.

[20] G.Q. Zhang, G.J. Hirasaki, W.V. House, Effect of internal field gradients on NMR measurements, Petrophysics 42 (2001) 37–47.

[21] K.R. Brownstein, C.E. Tarr, Importance of classical diffusion in NMR studies of water in biological cells, Phys. Rev. A 19 (1979) 2446.

[22] L. Marinelli, M.D. Hürlimann, P.N. Sen, Modal analysis of q-space–relaxation correlation experiments, J. Chem. Phys. 118 (2003) 8927–8940.

[23] D. van Dusschoten, C.T.W. Moonen, P.A. de Jager, H.V. As, Unraveling diffusion constants in biological tissue by combining Carr–Purcell–Meiboom–Gill imaging and pulsed field gradient NMR, Magn. Reson. Med. 36 (1996) 907–913.

[24] G.J. Stanisz, R.M. Henkelman, Diffusional anisotropy of T_2 components in bovine optic nerve, Magn. Reson. Med. 40 (1998) 405–410.

[25] S. Peled, D.G. Cory, S.A. Raymond, D.A. Kirschner, F.A. Jolensz, Water diffusion, T_2, and compartmentation in frog sciatic nerve, Magn. Reson. Med. 42 (1999) 911–918.

[26] L. Venkataramanan, Y. Song, M.D. Hürlimann, Solving Fredholm integrals of the first kind with tensor product structure in 2 and 2.5 dimensions, IEEE Trans. Signal Process. 50 (2002) 1017–1026.

[27] J.E. Tanner, Use of the stimulated echo in NMR diffusion studies, J. Chem. Phys. 52 (1970) 2523–2526.
[28] R.M. Weisskoff, C.S. Zuo, J.L. Boxerman, B.R. Rosen, Microscopic susceptibility variation and transverse relaxation: theory and experiment, Magn. Reson. Med. 31 (1994) 601.
[29] P.N. Sen, S. Axelrod, Inhomogeneity in local magnetic field due to susceptibility contrast, J. Appl. Phys. 86 (1999) 4548–4554.
[30] G.Q. Zhang, G.J. Hirasaki, W.V. House, Effect of internal field gradients on NMR measurements, Petrophysics 42 (2001) 37–47.